Article

4D-Flow MRI Characterization of Pulmonary Flow in Repaired Tetralogy of Fallot

Ashifa Hudani [1,2], Safia Ihsan Ali [1,2], David Patton [3,4], Kimberley A. Myers [3], Nowell M. Fine [4,5], James A. White [2,4,5], Steven Greenway [4,5,6,7] and Julio Garcia [2,4,5,6,8,*]

1   Department of Biomedical Engineering, University of Calgary, Calgary, AB T2N 1N4, Canada
2   Stephenson Cardiac Imaging Centre, University of Calgary, Calgary, AB T2N 1N4, Canada
3   Department of Pediatrics, Cumming School of Medicine, University of Calgary, Calgary, AB T2N 1N4, Canada
4   Department of Cardiac Sciences, Cumming School of Medicine, University of Calgary, Calgary, AB T2N 1N4, Canada
5   Libin Cardiovascular Institute, University of Calgary, Calgary, AB T2N 1N4, Canada
6   Alberta Children's Hospital Research Institute, University of Calgary, Calgary, AB T2N 1N4, Canada
7   Department of Biochemistry and Molecular Biology, Cumming School of Medicine, University of Calgary, Calgary, AB T2N 1N4, Canada
8   Department of Radiology, Cumming School of Medicine, University of Calgary, Calgary, AB T2N 1N4, Canada
*   Correspondence: julio.garciaflores@ucalgary.ca

Featured Application: Repaired Tetralogy of Fallot pulmonary hemodynamic alterations can be characterized by 4D-flow MRI.

Abstract: Patients with Tetralogy of Fallot (TOF) have multiple surgical sequelae altering the pulmonary flow hemodynamics. Repaired TOF (rTOF) adults frequently develop pulmonary regurgitation impacting the blood flow pressure, right ventricle load, and pulmonary hemodynamics. We aimed to evaluate the pulmonary flow hemodynamics using 4D-flow magnetic resonance imaging (MRI) for characterizing altered blood flow, viscous energy loss (EL), wall shear stress (WSS), pressure drop (PD), and ventricular flow analysis (VFA) in rTOF patients. We hypothesized that 4D-flow based parameters can identify pulmonary blood flow alterations. A total of 17 rTOF patients (age: 29 ± 10 years, 35% women) and 20 controls (age: 36 ± 12 years, 25% women) were scanned using a dedicated cardiac MRI protocol. Peak velocity and regurgitant fraction were significantly higher for rTOF patients ($p < 0.001$). WSS was consistently elevated along the PA in the rTOF ($p \leq 0.05$). The rTOF average circumferential WSS was higher than axial WSS at the main pulmonary artery ($p \leq 0.001$). PD and EL were consistently higher in the rTOF as compared with controls ($p < 0.05$). For VFA, delayed ejection increased and retained inflow decreased in rTOF patients ($p < 0.001$). To conclude, this study demonstrated that 4D-flow MRI pulmonary flow in the rTOF can exhibit altered peak velocity, valvular regurgitation, WSS, EL, PD, and VFA.

Keywords: 4D-flow MRI; repaired tetralogy of Fallot; pulmonary flow

1. Introduction

The most common cyanotic congenital heart defects (CHD) is Tetralogy of Fallot (TOF) [1]. It represents ~7% of congenital heart malformations and occurs in nearly 1 in 3500 births [2]. These heart defects include right ventricular (RV) hypertrophy, ventricular septal defect, pulmonary stenosis, and overriding aortic root [1]. However, given the advancement of comprehensive cardiovascular surgical techniques, these patients are able to undergo repair and survive until adulthood [3,4]. Even after repair, many patients require postoperative sequelae long-term surveillance, which includes right/left ventricular dysfunction, RV dilation or hypertrophy, residual RV outflow tract (RVOT) obstruction, and pulmonary regurgitation (PR) [1,5].

The evaluation of cardiovascular flow is commonly performed by Doppler echocardiography. However, this imaging modality is limited by many constraints including limited acoustic window, variable velocity assessment, and operator expertise [6,7]. In addition, the calculation of net flow and mean velocities is frequently based on assumptions (i.e., circularity and flow parabolic profile), resulting in inaccurate flow quantification in tortuous vessel geometries along with complex helical flow [6]. Thus, a more comprehensive and advanced evaluation is required for better understanding of repaired TOF (rTOF) patients.

Cardiovascular magnetic resonance (CMR) is currently used for monitoring rTOF patients when the pulmonary artery and RV are difficult to visualize and evaluate with Doppler echocardiography due to poor acoustic windows in retrosternal position [7,8]. The most frequently used flow sequence is two-dimensional phase-contrast (PC) CMR with through-plane velocity encoding (2D cine PC-CMR) [6]. Even though this technique is widely used for flow quantification, due to the underlying assumptions that are made, it is subject to various inaccuracies in eccentric jets and complex flow patterns. However, 4D-flow magnetic resonance imaging (MRI) measures the velocity in each spatial direction (x,y,z) throughout the cardiac cycle [9,10]. Furthermore, 4D-flow MRI facilitates off-line measurement of hemodynamic metrics anywhere within the data volume [9]. It provides exceptional visualization of complex flow patterns, hence it is increasingly being used and beneficial to guide surgical intervention such as Fontan conduit placement [4,10,11]. In addition, 4D-flow MRI derivates various hemodynamic parameters, enabling the quantification of wall shear stress (WSS), viscous energy loss (EL), pressure drop (PD), and ventricular flow analysis (VFA) [1,6,12]. Incremental helical or vortical flow in the main pulmonary artery (MPA) is characteristic of patients with rTOF [13–15]. Hence, further higher hemodynamic parameters need to be evaluated at the MPA to better understand the abnormal hemodynamics that are presented within patients with rTOF.

Therefore, this study aimed to investigate pulmonary hemodynamics using 4D-flow MRI for characterizing altered VFA, WSS, EL, and PD changes in rTOF patients. We hypothesize that 4D-flow-based parameters can identify pulmonary blood flow alterations.

2. Materials and Methods

2.1. Study Population

A total of 17 patients with rTOF and 20 controls were retrospectively recruited from the Cardiovascular Imaging Registry of Calgary (CIROC). Inclusion and exclusion criteria were summarized in Table 1 and follow current recommendations [16]. Prior to examination, baseline demographic measurements were collected. To capture the participant health status questionnaires, informed consent, and for the recording of MRI-related variables, CardioDI^{TM} was used (Cohesic Inc., Calgary, AB, Canada). This study was approved by the University of Calgary Research Ethics Board. All participants provided written consent at the MRI scan examination.

Table 1. Acquisition parameters for 4D-flow.

	Inclusion			Exclusion		
	Age > 18	**No History of CVD**	**No Hypertension**	**Record of Tetralogy of Fallot**	**Unable to Complete MRI**	**Poor Image Quality**	**Contra-Indication for MRI**
Controls	✔	✔	✔		✔	✔	✔
Patients	✔		✔	✔	✔	✔	✔

CVD: Cardiovascular Disease; MRI: Magnetic Resonance Imaging.

2.2. Cardiac MRI

A 3T MRI scanner (Skyra/Prisma, Siemens, Erlangen, Germany) was used on all subjects to perform a standard-of-care cardiac imaging study for congenital disease in accordance with expert recommendations [16]. The entire heart was imaged through segmented electrocardiogram (ECG) gating, time-resolved balanced steady-state free precision

(SSFP) [17]. Furthermore, 0.2 mmol/kg of gadolinium (Gadovist®, Bayer Inc., Mississauga, ON, Canada) was administered to acquire a contrast-enhanced magnetic resonance angiography (CE-MRA). To obtain the whole-heart in vivo volumetric blood flow, a 4D-flow MRI WIP was applied shortly after the administration of gadolinium, using free-breathing retrospective ECG-gating and an adaptative respiratory navigator as previously reported [17]. Basic acquisition parameters were summarized in Table 2. Variations in heart rate and navigator efficiency affected total scanning time (6–10 min).

Table 2. Acquisition parameters for 4D flow.

Bandwidth (Hz/Pixel)	Repetition Time (ms)	Echo Time (ms)	Spatial Resolution (mm³)	Phases	Temporal Resolution (ms)
455–495	4.53–5.07	2.01–2.35	2.0–3.6 × 2.0–3.0 × 2.5–3.5	30	25–35

2.3. Standard Cardiac Imaging Evaluation

Cine images were assessed using cvi^{42} 5.11.5 (Circle Cardiovascular Imaging Inc., Calgary, AB, Canada) by clinical blinded readers to determine left ventricle/right ventricle end-diastolic volume (LVEDV/RVEDV), end-systolic volume (LVESV, RVESV), and the ejection fraction (LVEF, RVEF). Pulmonary artery diameter assessment was performed using the acquired CE-MRA volume. Location planning was performed using multi-planar reformatting for the accurate visualization of the anatomical structure, Figure 1.
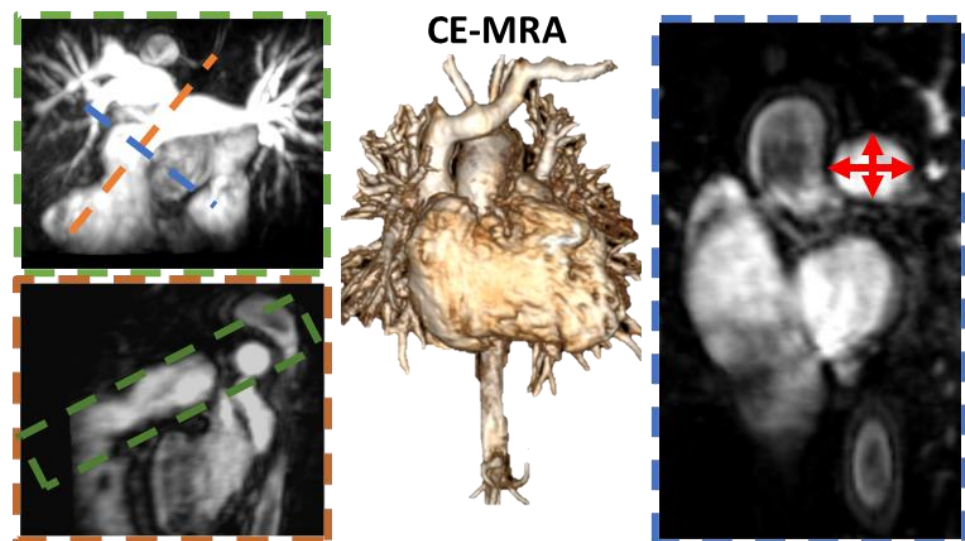

Figure 1. Pulmonary artery diameter measurement. Middle panel shows the contrast-enhanced magnetic resonance angiogram (CE-MRA) used to calculate the pulmonary artery (PA) diameter. For finding the appropriate mild PA location, multi-planar reconstruction (MPR) allowed us to freely navigate the volume, as it showed in the blue, green, and orange planes. An MPR maximum intensity projection was used for the green plane to accurately project the PA volume. Red arrows show samples of diameter measurements.

2.4. 4D-Flow Data Analysis

All analyses were conducted by a single investigator using a prototype 4D-flow module within cvi^{42} version 5.11.5. The workflow for the plane and volume analysis included: (1) Pre-processing corrections included, when it was needed, eddy currents, velocity aliasing, and static tissue, Figure 2A; (2) To segment the entire volume of the pulmonary artery (PA), the phase-contrast angiogram (PC-MRA) was divided into subvolumes including the main pulmonary artery (MPA), the right PA (RPA), and the left PA (LPA) for hemodynamic assessment; and (3) Six planes were placed along the PA at the

following positions: pre-pulmonic, pulmonic valve, mid-pulmonary, pre-bifurcation, and 1cm into both the left and right bifurcations, see Figure 2B. The following hemodynamic parameters were calculated at each plane position: total volume, peak velocity, regurgitant fraction, PD using pre-pulmonic plane as reference, WSS, and EL. Volume samples for WSS, PD, and EL are presented in Figure 2C–E.
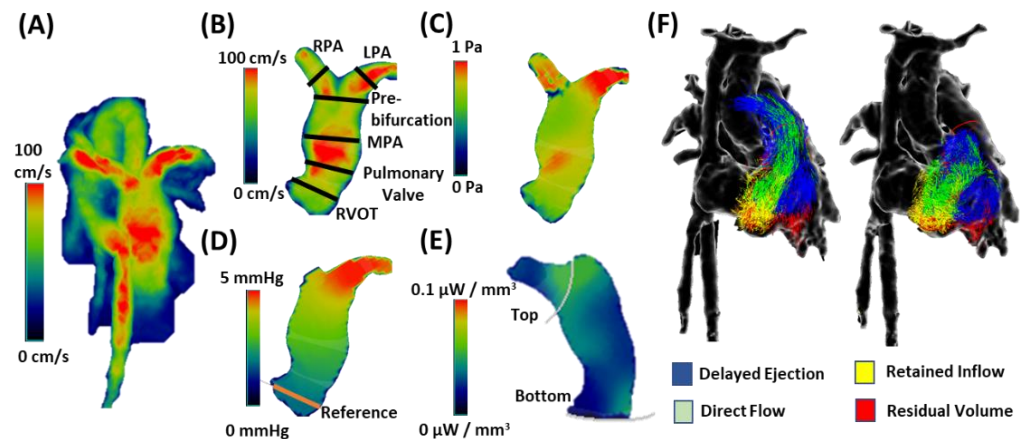
Figure 2. Post-processing of 4D-flow. First, 4D-flow velocity field (Vi, Vj, Vk) was corrected (Panel (**A**)). Followed by data correction, the pulmonary artery was segmented for regional analysis. Several analysis planes were placed at specific landmarks for blood hemodynamic assessment: right ventricular outflow tract (RVOT), pulmonary valve, main pulmonary artery (MPA), pre-bifurcation, right pulmonary artery (RPA), and left pulmonary artery (LPA). Panel (**B**,**C**) shows a sample of wall shear stress at peak systole. Pressure drop used the RVOT plane as reference location (Panel (**D**)). Energy loss used a centerline to guide a top and a bottom plane (grey lines) to define the volume of interest, (Panel (**E**)). Panel (**F**) illustrates a sample of ventricular flow analysis distribution components.

Then, VFA was performed by placing the inflow plane at the tricuspid valve and pulmonic valve. The flow area was manually traced on each valve plane at each phase of the cardiac cycle. The isovolumetric relaxation phase (right heart valves closed) at the end systole was used to release particles, characterizing the flow distribution. Four flow components of the right ventricle (RV) were obtained: direct flow (flow enters and exits from the RV), retained inflow (flow remaining in the RV), delayed ejection (part of the existing RV flow exiting the RV during ejection), and residual volume (flow entering the RV but retained for more than one cycle), see Figure 2F.

2.5. Statistical Analysis

IBM SPSS Statistics for Windows version 27 was used for analysis (IBM Corp., Armonk, NY, USA). At first, to evaluate if the data was normally distributed, a Shapiro–Wilk's test was performed for all parameters. Providing a normal distribution, an independent samples *t*-test was performed to identify any significant differences within the hemodynamic parameters presented between patients and controls. A *p*-value < 0.05 was considered statistically significant. Furthermore, Pearson's correlation was calculated between all hemodynamic parameters and the MPA diameter. A *p*-value < 0.01 was considered statistically significant.

3. Results

Subject baseline characteristics are reported in Table 3. The total population (*n* = 37) included 20 controls and 17 rTOF patients. Baseline age was higher in controls as compared with patients (38 ± 13 year vs. 29 ± 13 year, *p* = 0.022). PA diameter was larger in rTOF patients as compared with controls (34 ± 4 mm vs. 24 ± 4 mm, *p* < 0.001). As showed in Table 3, LVEF was similar in both groups ($60 \pm 4\%$ vs. $62 \pm 4\%$, *p* = 0.353), but indexed LV volumes were lower in patients as compared with controls: LVEDVi (77 ± 46 mL/m^2 vs. 111 ± 46 mL/m^2, *p* = 0.006) and LVESVi (31 ± 19 mL/m^2 vs. 42 ± 19 mL/m^2, *p* = 0.044).

RVEF was significantly reduced in rTOF patients ($46 \pm 3\%$ vs. $54 \pm 3\%$, $p < 0.001$), whereas RV volumes were higher in rTOF patients ($p < 0.05$). However, rTOF patients did not have severe RV dilation (RV/LV volume ratio ≥ 2.30).

**Table 3.** Baseline characteristics from cardiac magnetic resonance imaging.

	Patients ($n = 17$)	Controls ($n = 20$)	p-Value
Age at scan (year)	29 ± 13	38 ± 13	0.022
Sex (f/m)	6/11	6/14	0.740
BSA (m^2)	1.78 ± 0.26	1.92 ± 0.26	0.093
HR (bpm)	71 ± 12	64 ± 12	0.125
BP systolic (mmHg)	105 ± 15	110 ± 15	0.254
BP diastolic (mmHg)	59 ± 16	61 ± 16	0.571
Pulmonary diameter (mm)	34 ± 4	24 ± 4	<0.001
LVEF (%)	60 ± 4	62 ± 4	0.353
LVEDV (mL)	138 ± 47	140 ± 47	0.868
LVEDVi (mL/m^2)	77 ± 46	111 ± 46	0.006
LVESV (mL)	56 ± 19	54 ± 19	0.719
LVESVi (mL/m^2)	31 ± 19	42 ± 19	0.044
RVEF (%)	46 ± 3	54 ± 3	<0.001
RVEDV (mL)	231 ± 46	181 ± 46	0.054
RVEDVi (mL/m^2)	128 ± 20	92 ± 20	0.006
RVESV (mL)	128 ± 24	83 ± 24	0.012
RVESVi (mL/m^2)	71 ± 11	42 ± 11	0.003

BSA: Body Surface Area; BP: Blood Pressure; HR: Heart Rate; LVEF: Left Ventricular Ejection Fraction; LVEDV: Left Ventricular End Diastolic Volume; LVEDVi: Indexed Left Ventricular End Diastolic Volume; LVESVi: Indexed Left Ventricular End Systolic Volume; LVESV: Left Ventricular End Diastolic Volume; RVEF: Right Ventricular Ejection Fraction; RVEDVi: Indexed Right Ventricular End Diastolic Volume; RVESVi: Indexed Right Ventricular End Systolic Volume; RVEDV: Right Ventricular End Diastolic Volume; RVESV: Right Ventricular End Systolic Volume.

An example comparing velocity and flow patterns between a control and an rTOF patient is shown in Figure 3. Homogeneous velocity mapping and laminar flow are observed in the healthy control, Figure 3A. Anatomic differences in the rTOF patient can be observed in the MPA producing flow acceleration and unbalanced flow distribution in the RPA and LPA, shown in Figure 3B. The descending aorta also showed flow acceleration due to the development of aortic coarctation. Similarly, pathlines showed helical flow in both MPA and bifurcation, shown in Figure 3B.
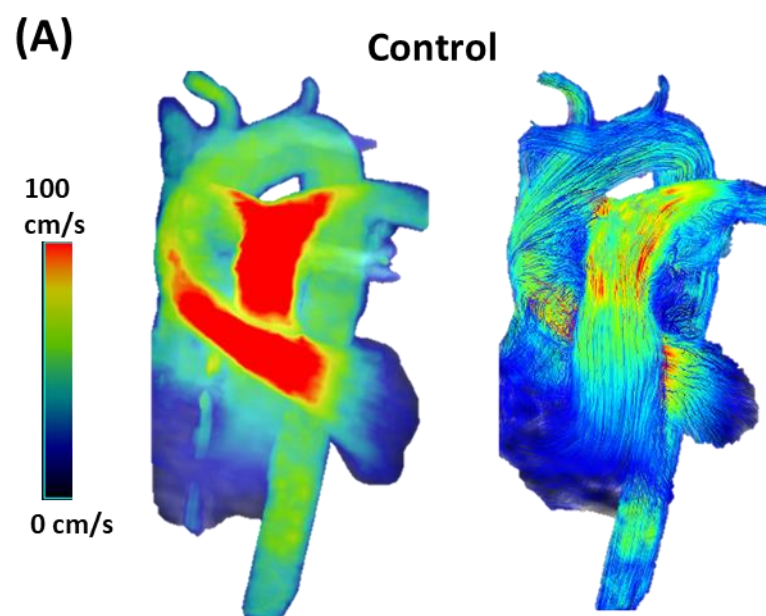

Figure 3. *Cont.*
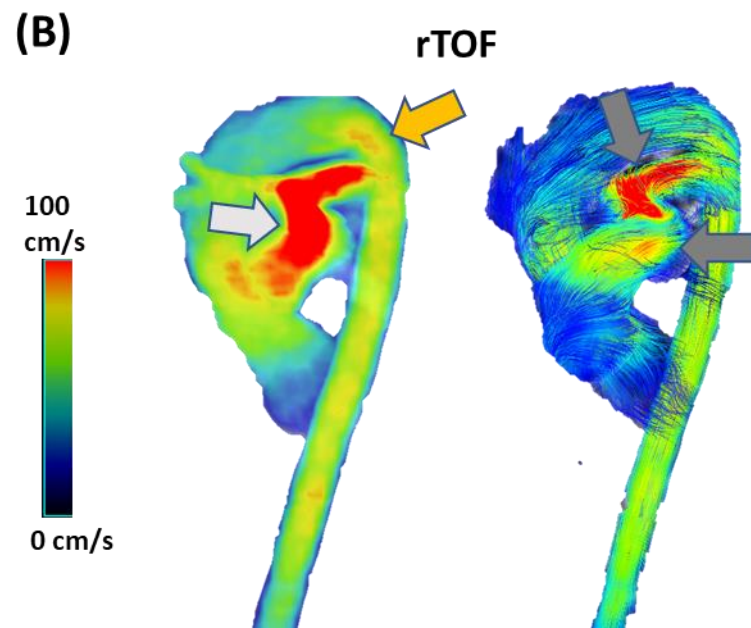
Figure 3. Comparison of velocity and flow patterns between a control and a patient with repaired Tetralogy of Fallow. Panel (**A**) shows homogeneous flow distribution in the velocity mapping (left) and laminar flow in the pulmonary artery and in the aorta (right). Panel (**B**) shows evidence of anatomic anomalies in the main pulmonary artery and aortic arch. These anomalies produced flow acceleration, as pointed by the light grey arrow in the pulmonary artery and the orange arrow in the aorta. Helical flow was also observed along the pulmonary artery, as pointed out by the dark grey arrows.

Figure 4 shows the 4D-flow assessment of total volume, peak velocity, and regurgitant fraction at the RVOT, pulmonary valve, MPA, RPA, and LPA. Total volume at the pulmonary valve was significantly elevated in the controls than in the rTOF ($54 \pm 18\%$ vs. $74 \pm 18\%$, $p = 0.001$, Figure 5A). In contrast, peak velocity and regurgitant fraction were significantly higher at all plane locations for the rTOF patients in comparison with the controls ($p < 0.001$, Figure 5B,C).
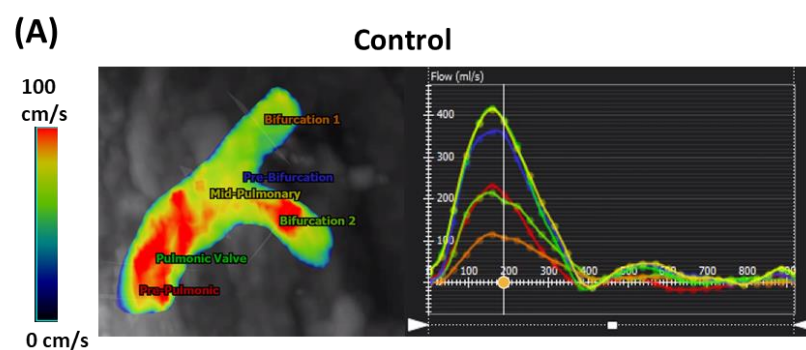
Figure 4. *Cont*.
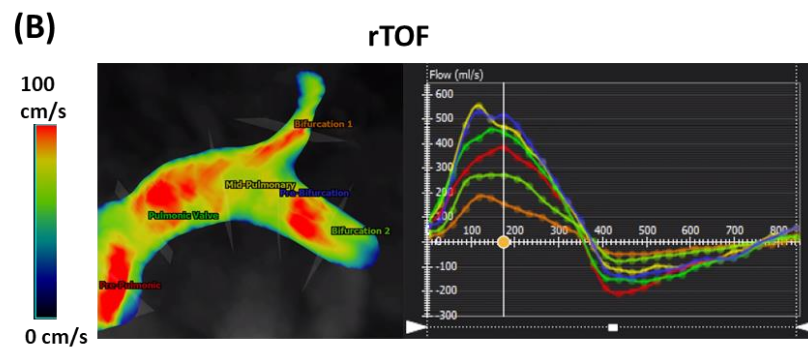
**Figure 4.** Plane planning and flow assessment along the pulmonary artery using 4D-flow. Velocity mapping is shown in the left and flow chart in the right. The vertical line indicates the phase in the cardiac cycle. Panel (**A**) illustrates the flow analysis of a healthy control. Each plane has an associated color in the flow chart. Panel (**B**) illustrates the flow analysis of a patient with repaired Tetralogy of Fallot. Remark that all planes measured some degree of flow regurgitation.
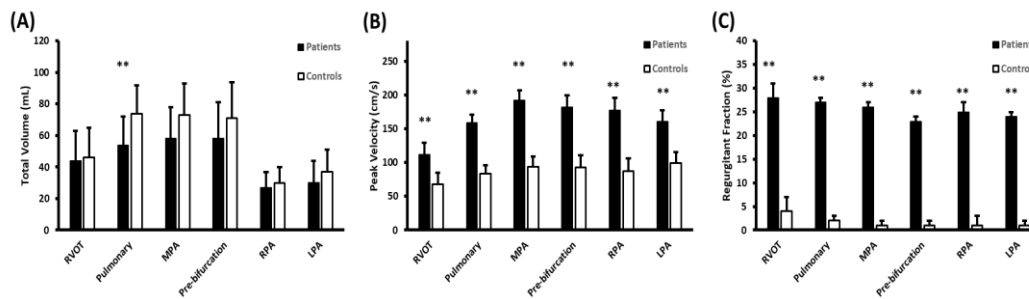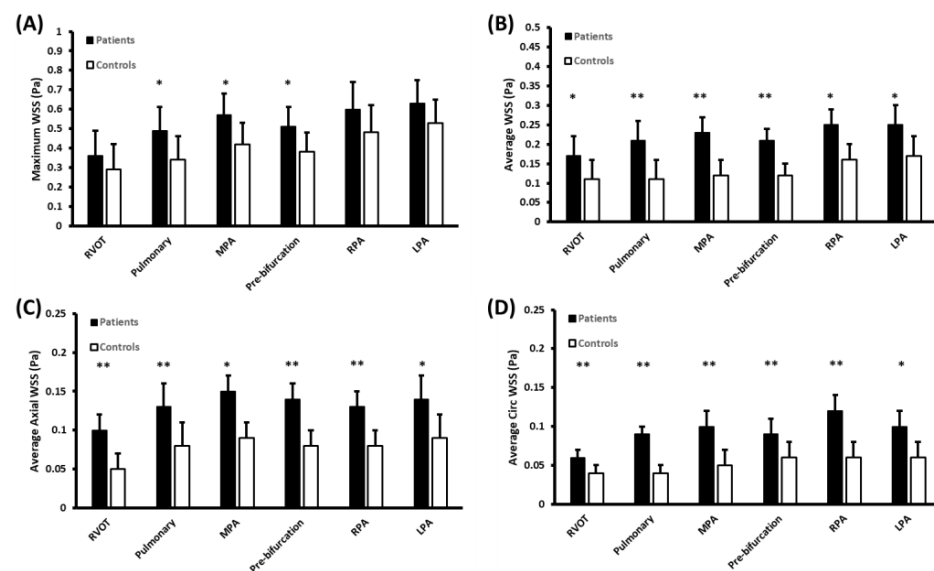

Figure 5. Plane hemodynamic assessment along the pulmonary artery using 4D flow. Right ventricular outflow tract (RVOT), pulmonary valve, main pulmonary artery (MPA), pre-bifurcation, right pulmonary artery (RPA), and left pulmonary artery (LPA). Panel (**A**) shows the assessment of total flow. Panel (**B**) shows the peak velocity assessment. Panel (**C**) shows the assessment of regurgitant fraction. ** indicates p-value ≤ 0.001 between rTOF patients and controls.

A comparison of WSS plane measurements between a control and a patient with rTOF is illustrated in Figure 6. Figure 7 presents the results of the WSS evaluation in all planes along the PA. Patients with rTOF showed an elevated maximum WSS at the pulmonary valve, MPA, and pre-bifurcation ($p \leq 0.05$). Average WSS was consistently elevated along the PA at all plane locations ($p \leq 0.05$). In line with maximum WSS, pulmonary valve, MPA, and pre-bifurcation showed greater differences with controls ($p \leq 0.001$). When assessing the vectorial WSS decomposition in axial and circumferential WSS at all plane locations, an elevation was found in rTOF patients ($p \leq 0.05$). In particular, the rTOF average circumferential WSS was higher than axial WSS at the MPA ($p \leq 0.001$).
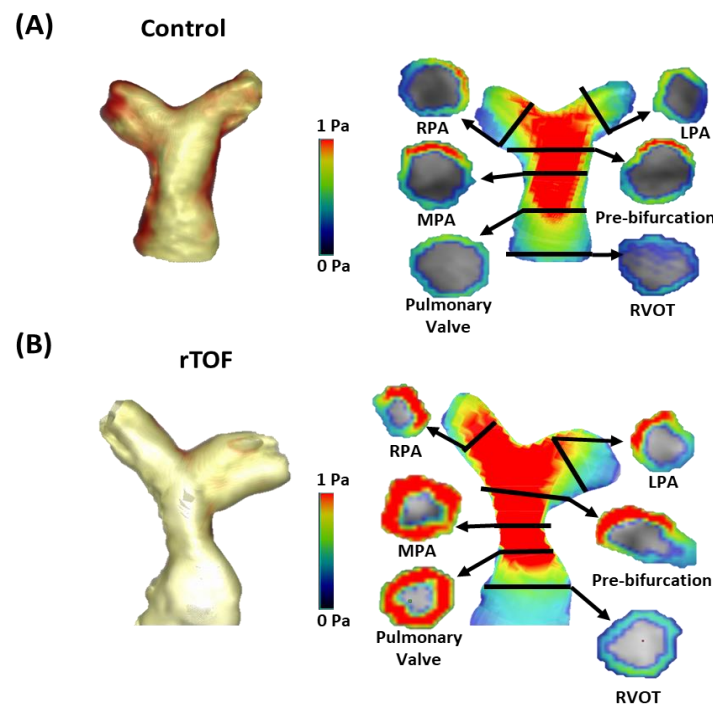
Figure 6. Wall shear stress analysis plane assessment along the pulmonary artery. Panel (**A**) shows the example of a healthy volunteer and Panel (**B**) shows the corresponding measurements for a patient with repaired Tetralogy of Fallot (rTOF). RVOT: right ventricle outflow tract; MPA: main pulmonary artery; RPA: right pulmonary artery; LPA: left pulmonary artery. Remark that the visualization threshold affects lumen thickness representation in the analysis software, but it does not impact the quantification.

Figure 7. Wall shear stress assessment along the pulmonary artery. Right ventricular outflow tract (RVOT), pulmonary valve, main pulmonary artery (MPA), pre-bifurcation, right pulmonary artery (RPA), and left pulmonary artery (LPA). Panel (**A**) shows the assessment of maximum wall shear stress (WSS). Panel (**B**) shows the average WSS assessment. Panel (**C**) shows the assessment of average axial WSS and Panel (**D**) shows the average circumferential (Circ) WSS. * indicates p-value ≤ 0.05 between rTOF patients and controls. ** indicates p-value ≤ 0.001 between rTOF patients and controls.

PD was consistently higher in the rTOF patients versus the controls ($p < 0.05$) along the PA, Figure 8. Maximum PD differences were more apparent in the pulmonary valve, MPA,

pre-bifurcation, and RPA. For average PD, the most noticeable difference was observed at the pulmonary valve plane.
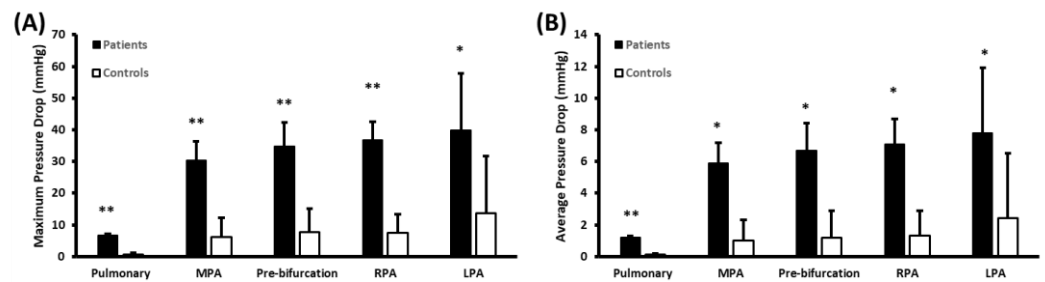
Figure 8. Pressure drops along the pulmonary artery. Pulmonary valve, main pulmonary artery (MPA), pre-bifurcation, right pulmonary artery (RPA), and left pulmonary artery (LPA). The right ventricular outflow tract was used as the reference plane location. Panel (**A**) shows the assessment of maximum pressure drop (PD). Panel (**B**) shows the average PD. * indicates *p*-value ≤ 0.05 between rTOF patients and controls. ** indicates *p*-value ≤ 0.001 between rTOF patients and controls.

Table 4 summarizes the correlations between analysis plane measurements and the pulmonary artery diameter, pulmonary valve peak velocity, and regurgitant fraction.

Table 4. Correlations with main pulmonary artery diameter, pulmonary valve peak velocity, and regurgitant fraction.

Parameter	MPA Diameter (r, *p*-Value)	Pulmonary Valve Peak Velocity (r, *p*-Value)	Pulmonary Valve Regurgitant Fraction (r, *p*-Value)
RVOT Peak Velocity	0.520, 0.002	0.474, 0.003	0.478, 0.003
RVOT Regurgitant Fraction	0.480, 0.005	0.487, 0.002	0.787, 0.001
Pulmonary Valve Peak Velocity	0.544, 0.001	-	0.316, 0.056
Pulmonary Valve Regurgitant Fraction	0.497, 0.004	0.316, 0.056	-
MPA Peak Velocity	0.564, 0.001	0.886, 0.001	0.310, 0.062
MPA Regurgitant Fraction	0.661, 0.001	0.520, 0.001	0.724, 0.001
Pre-bifurcation Peak Velocity	0.495, 0.004	0.898, 0.001	0.263, 0.116
Pre-bifurcation Regurgitant Fraction	0.624, 0.001	0.522, 0.001	0.862, 0.001
RPA Peak Velocity	0.181, 0.322	0.520, 0.001	0.288, 0.084
RPA Regurgitant Fraction	0.423, 0.016	0.448, 0.005	0.844, 0.001
LPA Peak Velocity	0.287, 0.111	0.673, 0.001	0.407, 0.012
LPA Regurgitant Fraction	0.679, 0.001	0.454, 0.005	0.873, 0.001
RVOT Average WSS	0.262, 0.147	0.230, 0.170	0.330, 0.046
Pulmonary Valve Average WSS	0.395, 0.025	0.361, 0.028	0.478, 0.003
MPA Average WSS	0.224, 0.218	0.475, 0.003	0.316, 0.057
Pre-bifurcation Average WSS	0.377, 0.033	0.617, 0.001	0.426, 0.009
RPA Average WSS	0.260, 0.150	0.550, 0.001	0.288, 0.084
LPA Average WSS	0.310, 0.084	0.726, 0.001	0.558, 0.001
Pre-bifurcation Maximum WSS	0.180, 0.325	0.405, 0.013	0.190, 0.260
RPA Maximum WSS	0.074, 0.689	0.522, 0.001	0.357, 0.030
LPA Maximum WSS	0.117, 0.522	0.384, 0.019	0.051, 0.763
RVOT Average axial WSS	0.340, 0.057	0.340, 0.039	0.570, 0.001
Pulmonary Valve Average axial WSS	0.364, 0.040	0.511, 0.001	0.506, 0.001
MPA Average axial WSS	0.421, 0.016	0.724, 0.001	0.492, 0.003
Pre-bifurcation Average axial WSS	0.401, 0.023	0.672, 0.001	0.593, 0.001
RPA Average axial WSS	0.409, 0.020	0.769, 0.001	0.485, 0.002
LPA Average axial WSS	0.395, 0.025	0.755, 0.001	0.228, 0.174
RVOT Average circumferential WSS	0.362, 0.042	0.732, 0.001	0.377, 0.021
Pulmonary Valve Average circumferential WSS	0.634, 0.001	0.870, 0.001	0.492, 0.002
MPA Average circumferential WSS	0.524, 0.002	0.725, 0.001	0.264, 0.114
Pre-bifurcation Average circumferential WSS	0.662, 0.001	0.639, 0.001	0.392, 0.016
RPA Average circumferential WSS	0.367, 0.039	0.744, 0.001	0.403, 0.013
LPA Average circumferential WSS	0.584, 0.001	0.725, 0.001	0.521, 0.001

PA: Pulmonary Artery; RVOT: Right Ventricle Outflow Tract; MPA: Main Pulmonary Artery; RPA: Right Pulmonary Artery; LPA: Left Pulmonary Artery; WSS: Wall Shear Stress.

Maximum EL was found significantly higher in the rTOF as compared to the controls along the PA (2.49 ± 0.23 mW vs. 0.37 ± 0.23 mW, $p < 0.001$). Most significant losses were observed at the pulmonary valve and bifurcation regions. The average EL was also found to be higher in the rTOF patients in comparison to controls (0.90 ± 0.11 mW vs. 0.15 ± 0.11 mW, $p < 0.001$). For VFA, delayed ejection showed a significant reduction in the rTOF patients versus the controls (20 ± 13% vs. 41 ± 13%, $p < 0.001$), and retained inflow showed a significant elevation in the rTOF patients when compared with the controls (32 ± 6% vs. 15 ± 6%, $p < 0.001$). A FVA comparison between a control and an rTOF patient is illustrated in Figure 9.
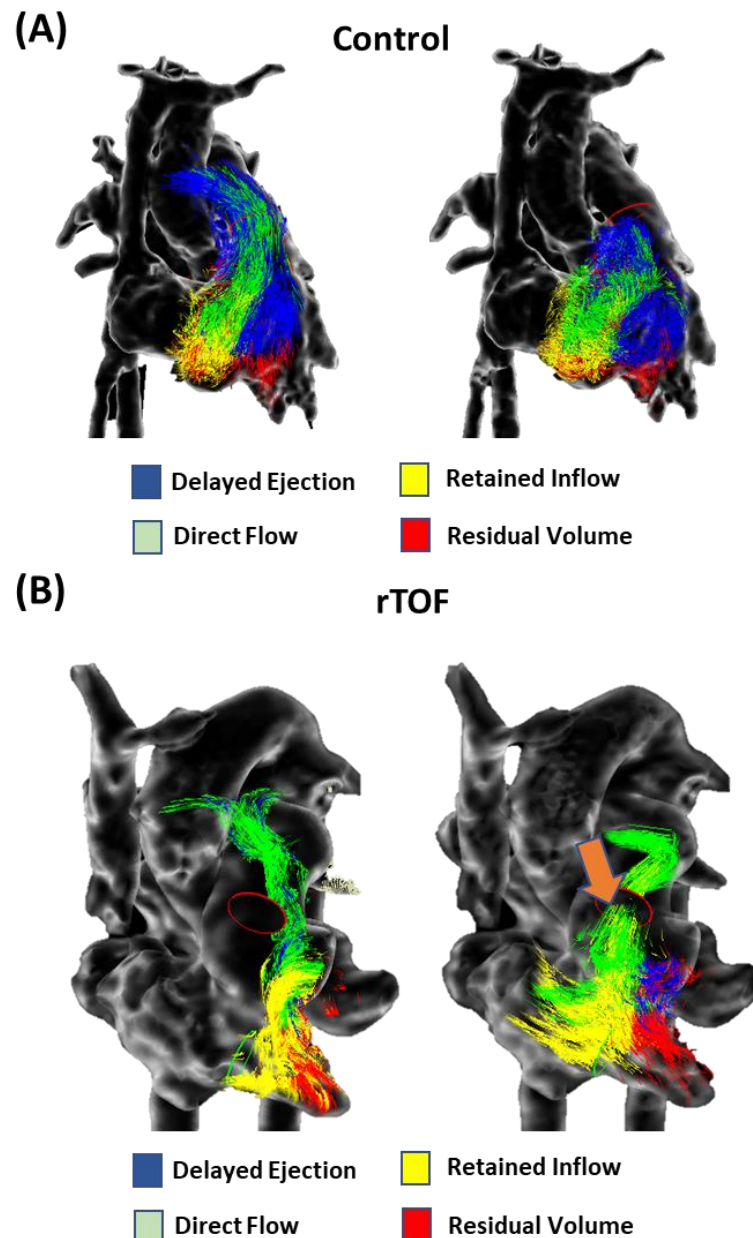
Figure 9. Comparison of ventricular flow analysis in a healthy control and a patient with repaired Tetralogy of Fallot. Panel (**A**) shows the ventricular flow analysis in a healthy control at peak systole (right) and early diastole (left). Panel (**B**) shows the ventricular flow analysis in a patient with repaired Tetralogy of Fallot (rTOF) with mild pulmonary regurgitation (orange arrow) at peak systole and early diastole.

Maximum and mean EL were also associated with the PA diameter (r = 0.645, $p < 0.001$ and r = 0.569, $p = 0.001$, respectively). Considering FVA, delayed ejection showed a negative association with PA diameter (r = −0.501, $p = 0.004$), whereas retained inflow showed an association (r = 0.502, $p = 0.003$).

Maximum and mean EL were also associated with the pulmonary valve peak velocity (r = 0.812, $p < 0.001$ and r = 0.914, $p < 0.001$, respectively). For VFA, pulmonary valve peak velocity was associated with delayed ejection (r = −0.507, $p = 0.001$) and retained inflow (r = 0.618, $p < 0.001$). Maximum and average valve pressure also showed a moderate association with the regurgitant fraction (r = 0.387, $p = 0.018$ and r = 0.333, $p = 0.044$, respectively). For maximum and average EL, the values were r = 0.354, $p = 0.032$ and r = 0.387, $p = 0.018$, respectively. For FVA, regurgitant fraction was negatively associated with delayed ejection (r = −0.478, $p = 0.003$) and retained inflow (r = 0.531, $p = 0.001$).

Right ventricular volumes and EF were associated with pulmonary regurgitant fraction: RVEDVi (r = 0.687, $p < 0.001$), RVESVi (r = 0.736, $p < 0.001$), and RVEF (r = −0.676, $p < 0.001$). Similarly, right ventricular volumes and EF were associated with maximum and average EL: RVEDVi (r = 0.404, $p = 0.027$ and r = 0.421, $p = 0.020$, respectively), RVESVi (r = 0.01, $p = 0.028$ and r = 0.405, $p = 0.026$), and RVEF (r = −0.435, $p = 0.016$ and r = −0.379, $p = 0.039$). For FVA, right ventricular volumes and EF were associated with delayed ejection and retained inflow: RVEDVi (r = −0.531, $p = 0.003$ and r = 0.668, $p < 0.001$, respectively), RVESVi (r = −0.554, $p = 0.002$ and r = 0.685, $p < 0.001$), and RVEF (r = 0.478, $p = 0.008$ and r = −0.516, $p = 0.004$).

4. Discussion

Our main findings derived from the 4D-flow MRI assessment and showed that: (1) peak velocity and regurgitant fraction are elevated in the rTOF with respect to the controls; (2) Axial and circumferential WSS demonstrated better discrimination between the rTOF and the controls than the WSS magnitude; (3) PD and EL were significantly higher in the rTOF in comparison to the controls; (4) VFA demonstrated a reduced delay ejection and an elevated retained flow on the rTOF as compared with the controls; and (6) PA diameter, pulmonary peak velocity, and right ventricular function were associated, in diverse degrees, to 4D-flow derived metrics. This study demonstrated that rTOF patients exhibited altered hemodynamics in the right heart as characterized by peak velocity, regurgitant fraction, WSS, EL, PD, and VFA using 4D-flow MRI.

The RV functional assessment can be challenging in the rTOF due to the dyssynchronous contraction patterns and anatomic complexity present in these patients. As expected, RV function was found to be slightly impaired in the rTOF cohort. In the present study, total volume, peak velocity, and regurgitant fraction succeeded in identifying local differences along the PA. A study performed on rTOF by van der Hulst et al. showed that 4D-flow plane measurements are more accurate than single direction 2D phase contrast for valvular flow and assessment of RV diastolic function [18]. Our results showed that 4D-flow can retrospectively assess standard flow metrics at any heart location. The latter has also been highlighted by the current recommendations for congenital heart diseases using 4D-flow MRI [10]. An important aspect of standard flow measurements at valve locations is valve tracking [19]. In the present study, we did not use valve tracking at the valve locations. However, recent studies have demonstrated that 4D-flow valve plane retrospective tracking can make the flow assessment more accurate by reducing errors in through-plane motion and flow angulation [10,19,20].

It is common in patients with rTOF to observe varying degrees of pulmonary regurgitation, pulmonary valve stenosis, PA branch stenosis, and PA dilation. Therefore, PA flow is expected to show some level of abnormalities. Previous work investigated the development of abnormal blood flow patterns in the RV and PA in the rTOF [4,14,21]. They reported helical flow and vortex formation in the RV and in the PA of the rTOF. Gbinigies et al. showed counter-rotating helical streams along the MPA and its association at peak systole with helical flow observed at the bifurcations [22]. The development of helical flow is not

well understood. It has been suggested that it may be a response for driving the blood flow efficiently in the presence of stenosis in the vessel [23]. However, it can also be a physical adaptation due to characteristics of stenosis. We did not assess or quantify blood flow helicity or vorticity. Instead, we concentrated on understanding WSS, EL, and PD effects. There are few studies investigating the role of WSS in the rTOF. Our findings supported new evidence demonstrating that WSS magnitude was able to discriminate abnormal WSS along the PA. Our findings aligned with the results reported by Hu et al. [1]. Of particular interest, WSS vector decomposition (axial and circumferential WSS) demonstrated the capacity to detect abnormalities. Axial and circumferential WSS would be useful to explain the wall interactions with helical flow and vortex formation in future studies. In addition, WSS measurement showed varying degrees of correlation with PA diameter, pulmonary valve peak velocity, and regurgitant fraction supporting its potential clinical usefulness.

PD is currently calculated using 2D phase-contrast measurements by applying the simplified Bernoulli's equation. Falahatpisheh et al. showed that the simplified Bernoulli method underestimated PD throughout all cardiac phases and it is necessary to consider the entire velocity field and unsteady conditions [24]. In our study, maximum and average PD were significantly higher in the PA of the rTOF. There is limited literature on the assessment of 4D-flow-based PD along the PA in the rTOF. However, extensive literature exists in the context of aortic valve disease and aortopathies [25–27]. PD is a familiar measure for clinicians as the concept aligns with Doppler echocardiography assessment. A particular detail in the evaluated rTOF cohort was the consistent PD elevation along the PA. The LPA PD was found to be the higher for all analysis planes. The latter may be due to stenosis branching that is recurrent in rTOF patients.

Another interesting aspect of our study was the evaluation of EL. Energetic expenditure can provide insightful information about the hemodynamic performance and load coupling with the RV. As expected, the rTOF had a significant expenditure of EL in the PA. Other studies have explored the energetic cost of using kinetic energy instead of EL. Robinson et al. also demonstrated an increase in kinetic energy along the MPA in the rTOF as compared to controls across the cardiac cycle with a *p*-value < 0.01 [28]. However, important differences exist between kinetic energy and EL. Kinetic energy is given by $0.5 \times mV^2$, where *m* is the mass and *V* is the velocity. Kinetic energy represents the energy of an object because of its motion. EL basically reflects the viscous energy dissipation [29]. In our study, EL was found to be associated with pulmonary peak velocity, which is expected as peak velocity increasing the energetic dissipation.

One of the novel findings of this study was the assessment of VFA. Delayed ejection and retained inflow were able to characterize the intra-cardiac hemodynamic characteristics of rTOF patients. In addition, both parameters were associated with ventricular volumes and EF. The latter provided new information about the performance of the RV. As the baseline measurements indicated, it was a small impairment of the RV function. It was mostly identified by the RVEF. Both FVA components (delayed ejection and retained inflow) showed a better discrimination of RV performance than RV volumes and detected differences were higher than RV EF. Unfortunately, there is a limited literature on VFA in the rTOF.

The main limitation of this study was the cohort size, which included a total of *n* = 37 subjects. Another limitation was that a single investigator performed the data analysis. In this study, the age at surgical repair was not considered as a determinant factor for altered hemodynamics given that it was not possible to evaluate if it had an impact on adult hemodynamics. The age difference between controls and patients is also an important limitation of the study, as age and sex matching were not considered during recruitment. The presence of angular variations between the RVOT and the MPA and assessment of wall thickness were not evaluated. Despite this limitation, results showed clear differences and associations between the cohorts and evaluated parameters.

5. Conclusions

This study demonstrated that pulmonary flow hemodynamics in the rTOF can exhibit altered peak velocity, valvular regurgitation, WSS, EL, PD, and VFA. The advanced 4D-flow derived parameters were prone to identify flow abnormalities in the right heart of the rTOF. The latter may be useful to better characterize acquired disease development after repair and support preventive treatment to maintain normal RV function.

Author Contributions: Conceptualization A.H., S.I.A. and J.G.; methodology, A.H., S.I.A., D.P., K.A.M. and J.G.; validation, A.H., S.I.A., D.P., K.A.M., N.M.F., J.A.W., S.G. and J.G.; formal analysis, A.H. and J.G.; investigation, A.H., S.I.A., S.G. and J.G.; resources, S.G. and J.G.; data curation, A.H. and J.G.; writing—original draft preparation, A.H., S.I.A. and J.G.; writing—review and editing, A.H., S.I.A., D.P., K.A.M., N.M.F., S.G., J.A.W. and J.G.; visualization, A.H. and J.G.; supervision, S.G. and J.G.; project administration, J.G.; funding acquisition, S.G. and J.G. All authors have read and agreed to the published version of the manuscript.

Institutional Review Board Statement: The study was conducted according to the Declaration of Helsinki. CIROC (REB13-0902) was approved by the Conjoint Health Research Ethics Board of University of Calgary.

Informed Consent Statement: All subjects provided written informed consent.

Data Availability Statement: The anonymized data are available upon request from the corresponding author.

References

1. Hu, L.; Ouyang, R.; Sun, A.; Wang, Q.; Guo, C.; Peng, Y.; Qin, Y.; Zhang, Y.; Xiang, Y.; Zhong, Y. Pulmonary artery hemodynamic assessment of blood flow characteristics in repaired tetralogy of Fallot patients versus healthy child volunteers. *Quant. Imaging Med. Surg.* **2020**, *10*, 921–933. [CrossRef]

2. Villafañe, J.; Feinstein, J.A.; Jenkins, K.J.; Vincent, R.N.; Walsh, E.P.; Dubin, A.M.; Geva, T.; Towbin, J.A.; Cohen, M.S.; Fraser, C.; et al. Hot Topics in Tetralogy of Fallot. *J. Am. Coll. Cardiol.* **2013**, *62*, 2155–2166. [CrossRef]

3. Cuypers, J.A.; Menting, M.E.; Konings, E.E.; Opić, P.; Utens, E.M.; Helbing, W.A.; Witsenburg, M.; Bosch, A.E.V.D.; Ouhlous, M.; van Domburg, R.T.; et al. Unnatural History of Tetralogy of Fallot. *Circulation* **2014**, *130*, 1944–1953. [CrossRef]

4. François, C.J.; Srinivasan, S.; Schiebler, M.L.; Reeder, S.B.; Niespodzany, E.; Landgraf, B.R.; Wieben, O.; Frydrychowicz, A. 4D cardiovascular magnetic resonance velocity mapping of alterations of right heart flow patterns and main pulmonary artery hemodynamics in tetralogy of Fallot. *J. Cardiovasc. Magn. Reson.* **2012**, *14*, 16. [CrossRef]

5. Gatzoulis, M.A.; Balaji, S.; A Webber, S.; Siu, S.C.; Hokanson, J.S.; Poile, C.; Rosenthal, M.; Nakazawa, M.; Moller, J.H.; Gillette, P.C.; et al. Risk factors for arrhythmia and sudden cardiac death late after repair of tetralogy of Fallot: A multicentre study. *Lancet* **2000**, *356*, 975–981. [CrossRef]

6. Dyverfeldt, P.; Bissell, M.; Barker, A.J.; Bolger, A.F.; Carlhäll, C.-J.; Ebbers, T.; Francios, C.J.; Frydrychowicz, A.; Geiger, J.; Giese, D.; et al. 4D flow cardiovascular magnetic resonance consensus statement. *J. Cardiovasc. Magn. Reson.* **2015**, *17*, 1–19. [CrossRef]

7. Lai, W.W.; Gauvreau, K.; Rivera, E.S.; Saleeb, S.; Powell, A.J.; Geva, T. Accuracy of guideline recommendations for two-dimensional quantification of the right ventricle by echocardiography. *Int. J. Cardiovasc. Imaging* **2008**, *24*, 691–698. [CrossRef]

8. Jeong, D.; Anagnostopoulos, P.V.; Roldan-Alzate, A.; Srinivasan, S.; Schiebler, M.; Wieben, O.; François, C.J. Ventricular kinetic energy may provide a novel noninvasive way to assess ventricular performance in patients with repaired tetralogy of Fallot. *J. Thorac. Cardiovasc. Surg.* **2014**, *149*, 1339–1347. [CrossRef]

9. Stankovic, Z.; Allen, B.D.; Garcia, J.; Jarvis, K.B.; Markl, M. 4D flow imaging with MRI. *Cardiovasc. Diagn. Ther.* **2014**, *4*, 173–192. [CrossRef]

10. Zhong, L.; Schrauben, E.M.; Garcia, J.; Uribe, S.; Grieve, S.M.; Elbaz, M.S.; Barker, A.J.; Geiger, J.; Nordmeyer, S.; Marsden, A.; et al. Intracardiac 4D Flow MRI in Congenital Heart Disease: Recommendations on Behalf of the ISMRM Flow & Motion Study Group. *J. Magn. Reson. Imaging* **2019**, *50*, 677–681. [CrossRef]

11. Warmerdam, E.G.; Neijzen, R.L.; Voskuil, M.; Leiner, T.; Grotenhuis, H.B. Four-dimensional flow CMR in tetralogy of fallot: Current perspectives. *Br. J. Radiol.* **2022**, *95*, 20210298. [CrossRef]

12. Zhao, X.; Hu, L.; Leng, S.; Tan, R.-S.; Chai, P.; Bryant, J.A.; Teo, L.L.S.; Fortier, M.V.; Yeo, T.J.; Ouyang, R.Z.; et al. Ventricular flow analysis and its association with exertional capacity in repaired tetralogy of Fallot: 4D flow cardiovascular magnetic resonance study. *J. Cardiovasc. Magn. Reson.* **2022**, *24*, 1–17. [CrossRef]

13. Tsuchiya, N.; Nagao, M.; Shiina, Y.; Miyazaki, S.; Inai, K.; Murayama, S.; Sakai, S. Circulation derived from 4D flow MRI correlates with right ventricular dysfunction in patients with tetralogy of Fallot. *Sci. Rep.* **2021**, *11*, 11623. [CrossRef]

14. Hirtler, D.; Garcia, J.; Barker, A.; Geiger, J. Assessment of intracardiac flow and vorticity in the right heart of patients after repair of tetralogy of Fallot by flow-sensitive 4D MRI. *Eur. Radiol.* **2016**, *26*, 3598–3607. [CrossRef]

15. Schäfer, M.; Barker, A.J.; Morgan, G.J.; Jaggers, J.; Stone, M.L.; Browne, L.P.; Ivy, D.D.; Mitchell, M.B. Increased systolic vorticity in the left ventricular outflow tract is associated with abnormal aortic flow formations in Tetralogy of Fallot. *Int. J. Cardiovasc. Imaging* **2020**, *36*, 691–700. [CrossRef]

16. Kramer, C.M.; Barkhausen, J.; Bucciarelli-Ducci, C.; Flamm, S.D.; Kim, R.J.; Nagel, E. Standardized cardiovascular magnetic resonance imaging (CMR) protocols: 2020 update. *J. Cardiovasc. Magn. Reason.* **2020**, *22*, 17. [CrossRef]

17. Hudani, A.; White, J.A.; Greenway, S.C.; Garcia, J. Whole-Heart Assessment of Turbulent Kinetic Energy in the Repaired Tetralogy of Fallot. *Appl. Sci.* **2022**, *12*, 10946. [CrossRef]

18. Van der Hulst, A.E.; Westenberg, J.J.M.; Kroft, L.J.M.; Bax, J.J.; Blom, N.A.; de Roos, A.; Roest, A.A.W. Tetralogy of Fallot: 3D Velocity-encoded MR Imaging for Evaluation of Right Ventricular Valve Flow and Diastolic Function in Patients after Correction. *Radiology* **2010**, *256*, 724–734. [CrossRef]

19. Garcia, J.; Beckie, K.; Hassanabad, A.F.; Sojoudi, A.; White, J.A. Aortic and mitral flow quantification using dynamic valve tracking and machine learning: Prospective study assessing static and dynamic plane repeatability, variability and agreement. *JRSM Cardiovasc. Dis.* **2021**, *10*, 204800402199990. [CrossRef]

20. Warmerdam, E.; Krings, G.J.; Leiner, T.; Grotenhuis, H.B. Three-dimensional and four-dimensional flow assessment in congenital heart disease. *Heart* **2020**, *106*, 421–426. [CrossRef]

21. Geiger, J.; Callaghan, F.M.; Burkhardt, B.E.U.; Buechel, E.R.V.; Kellenberger, C.J. Additional value and new insights by four-dimensional flow magnetic resonance imaging in congenital heart disease: Application in neonates and young children. *Pediatr. Radiol.* **2021**, *51*, 1503–1517. [CrossRef]

22. Gbinigie, H.; Coats, L.; Parikh, J.D.; Hollingsworth, K.G.; Gan, L. A 4D flow cardiovascular magnetic resonance study of flow asymmetry and haemodynamic quantity correlations in the pulmonary artery. *Physiol. Meas.* **2021**, *42*, 025005. [CrossRef]

23. Liu, X.; Sun, A.; Fan, Y.; Deng, X. Physiological Significance of Helical Flow in the Arterial System and its Potential Clinical Applications. *Ann. Biomed Eng.* **2015**, *43*, 3–15. [CrossRef]

24. Falahatpisheh, A.; Rickers, C.; Gabbert, D.; Heng, E.L.; Stalder, A.; Kramer, H.-H.; Kilner, P.J.; Kheradvar, A. Simplified Bernoulli's method significantly underestimates pulmonary transvalvular pressure drop. *J. Magn. Reson. Imaging* **2015**, *43*, 1313–1319. [CrossRef]

25. Garcia, J.; Barker, A.J.; Markl, M. The Role of Imaging of Flow Patterns by 4D Flow MRI in Aortic Stenosis. *JACC Cardiovasc. Imaging* **2019**, *12*, 252–266. [CrossRef]

26. Hassanabad, A.F.; Burns, F.; Bristow, M.S.; Lydell, C.; Howarth, A.G.; Heydari, B.; Gao, X.; Fedak, P.W.; White, J.A.; Garcia, J. Pressure drop mapping using 4D flow MRI in patients with bicuspid aortic valve disease: A novel marker of valvular obstruction. *Magn. Reson. Imaging* **2019**, *65*, 175–182. [CrossRef]

27. Geeraert, P.; Jamalidinan, F.; Hassanabad, A.F.; Sojoudi, A.; Bristow, M.; Lydell, C.; Fedak, P.W.; White, J.A.; Garcia, J. Bicuspid aortic valve disease is associated with abnormal wall shear stress, viscous energy loss, and pressure drop within the ascending thoracic aorta. *Medicine* **2021**, *100*, e26518. [CrossRef]

28. Robinson, J.D.; Rose, M.J.; Joh, M.; Jarvis, K.; Schnell, S.; Barker, A.J.; Rigsby, C.K.; Markl, M. 4-D flow magnetic-resonance-imaging-derived energetic biomarkers are abnormal in children with repaired tetralogy of Fallot and associated with disease severity. *Pediatr. Radiol.* **2018**, *49*, 308–317. [CrossRef]

29. Barker, A.J.; van Ooij, P.; Bandi, K.; Garcia, J.; Albaghdadi, M.; McCarthy, P.; Bonow, R.O.; Carr, J.; Collins, J.; Malaisrie, S.C.; et al. Viscous energy loss in the presence of abnormal aortic flow. *Magn. Reson. Med.* **2013**, *72*, 620–628. [CrossRef]